# Energy loss of $^{14}N$ ions in Ni, Ag, and Cu and the lifetimes of the states at 2.3 and 3.9 MeV in $^{14}N$

M. Zielinski, W. Y. Baek, K. Bharuth-Ram,* D. Gassen, and W. Neuwirth
*I. Physikalisches Institut, University of Cologne, Federal Republic of Germany*
(Received 24 July 1987)

The energy loss of $^{14}N$ ions in Ni, Ag, and Cu has been investigated via the inverted Doppler-shift attenuation technique in the energy range up to 3.1 MeV. Excited $^{14}N$ nuclei were produced in the reaction $^{12}C(^3He,p)^{14}N^*$, and energy-loss information was obtained from the analysis of the Doppler-broadened 2.313-MeV $\gamma$-ray line, observed with a Ge(Li) detector. This analysis also yielded the lifetimes of the levels at 2.3 and 3.9 MeV in $^{14}N$, which were determined to be $97.7\pm5.5$ and $5.6\pm1.1$ fs, respectively, in reasonable agreement with previous measurements and theoretical calculations. The stopping cross sections obtained for all three stopping media are compared with existing theoretical calculations, especially with regard to the oscillations with the atomic number of the stopping medium.

## I. INTRODUCTION

The energy loss of $^{14}N$ projectiles in different materials has been previously investigated in a large energy range by Porat *et al.*[1] and by Neshev *et al.*[2] The former obtained the differential energy loss $dE_p/dx$ from measurements of the change in energy of the projectiles after transmission through thin foils, while the latter obtained relative stopping cross sections from measurements on backscattered projectiles, which were then converted to absolute values by normalization to the data of Porat at $v=0.020c$. The data of Neshev, however, are below the values of Porat at lower velocities and above those at higher velocities.

In this paper we report on our investigations of the energy loss of $^{14}N$ ions of velocities up to $v=0.022c$ in Ni, Cu, and Ag *via* the inverted Doppler-shift attenuation (IDSA) technique.[3,4] The IDSA technique exploits the dependence of the Doppler-broadened $\gamma$-ray line shapes on the velocity distribution of the projectiles, which have to be produced in an excited nuclear state. This velocity distribution is determined by the differential energy loss of the nuclei and the lifetime of the excited state (see Sec. II). If the lifetime of the excited state is known, an exact analysis of the Doppler spectra yields directly the absolute values of the differential energy loss of the projectiles; if it is unknown, relative values are obtained. In order to get this information it is necessary to consider all those effects which influence the shape of Doppler spectra: the finite energy resolution of the detector as well as its finite solid angle, and the angle straggling of the $^{14}N$ projectiles in the targets. Since these effects have particular relevance on the determination of nuclear lifetimes by the Doppler-shift attenuation (DSA) method, we have considered them at some length, and present the details in Sec. IV.

The stopping cross sections of the different media for $^{14}N$ ions were obtained from the analysis of the Doppler-broadened $\gamma$-ray line emitted from the first excited state of $^{14}N$ at 2.3 MeV. Its Doppler spectrum can be obtained in two different ways: first, by observing the $\gamma$-ray quanta in coincidence with protons produced in the direct population of the 2.3-MeV level, and second, indirectly, by observing $\gamma$-ray quanta in coincidence with protons emitted in the population of the 3.9-MeV level, which decays with a probability of 96% to the 2.3-MeV level (see Fig. 1).

Unfortunately, the lifetimes of these two states, which have to be known to derive absolute values of the stopping cross sections, show quite a scatter ($\pm30\%$) about

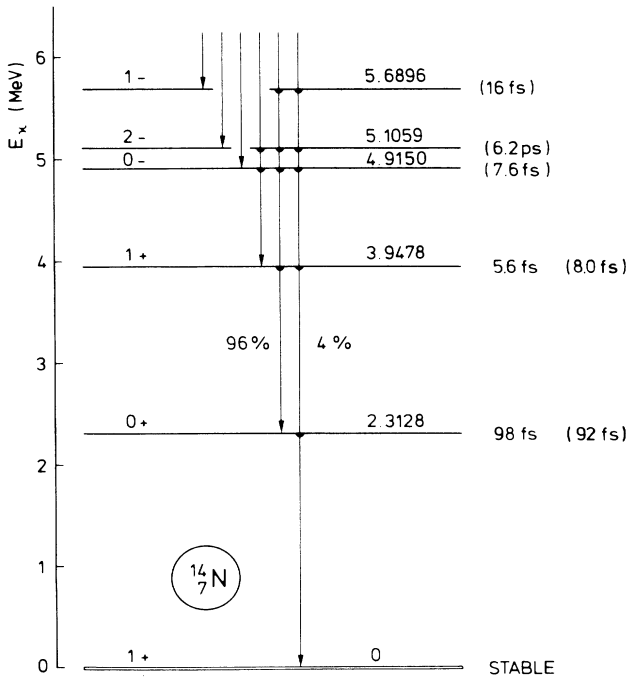


FIG. 1. Level scheme of $^{14}N$. Lifetimes in brackets and energies are from Ref. 5. The lifetimes given for the first and second excited state are the results of this work.

 

their mean values[5] of $\tau_1$ (2.3 MeV)=92 fs and $\tau_2$ (3.9 MeV)=8.0 fs. For $^{14}$N in Ni and Ag, however, there exist rather precise values of the stopping cross sections[1] in the relevant velocity region, which can be used to reevaluate the lifetimes of these states with a higher precision. These data have then been used to determine the stopping cross section of Cu.

## II. PRINCIPLES OF THE IDSA TECHNIQUE

The Doppler-broadened line shapes of $\gamma$ rays have been described by several authors (see, e.g., the references listed in the review by Nolan *et al.*[6]). Here we present only those aspects relevant to our method of extracting energy-loss information from an analysis of $\gamma$-ray line shapes.

The $\gamma$ rays emitted by excited $^{14}$N nuclei, which are produced in the reaction $^{12}$C($^3$He,$p$)$^{14}$N* and recoil into vacuum with start velocity $v_0$, are shifted in energy by the Doppler effect

$$E = E_0 \frac{[1-(v/c)]^{1/2}}{1-(v/c)\cos\vartheta} , \tag{1}$$

where $E_0$ is the $\gamma$-ray energy in the rest frame of the projectile, and $\vartheta$ is the angle between the direction of the projectile and that of the $\gamma$-ray emission. (In the remaining text the letter $E$ refers always to the $\gamma$-ray energy, the kinetic energy of the projectile is denoted by $E_p$.)

When the $\gamma$ rays are detected in coincidence with the corresponding protons emitted in a certain direction, the start velocity $v_0$ and the direction of the $^{14}$N projectiles are uniquely determined by the reaction kinematics. The $\gamma$-ray-emission angle $\vartheta$ of the observed $\gamma$-ray quanta would be fixed, too, if the solid angle of the $\gamma$-ray detector could be made very small, which, however, was not possible. In order to obtain a reasonable count rate of coincidences a solid angle of 0.18 sr was chosen. According to Eq. (1), the spread in the accepted $\gamma$-ray-emission angles $\vartheta$ gives a finite distribution in the observed unattenuated $\gamma$-ray spectrum even for projectiles moving through vacuum, which can—in an axially symmetric geometry—be described by

$$\frac{dN_u}{dE} = N_0 F(\vartheta) \left| \frac{d\vartheta(v_0,E)}{dE} \right| . \tag{2}$$

The $\gamma$ rays emitted by excited nuclei, which are slowed down in matter, exhibit an attenuated Doppler shift, which depends on the velocity at the moment of emission of the $\gamma$-ray quanta. The $\gamma$-ray-emission rate at a given time $t(v)$ is determined by the decay law, which is the normal exponential function; if the state at 2.3 MeV with lifetime $\tau_1$ is directly excited,

$$\frac{dN}{dt} = \frac{N_0}{\tau_1} \exp[-t(v)/\tau_1] . \tag{3a}$$

The decay rate for the case of excitation via feeding from the higher state at 3.9 MeV with lifetime $\tau_2$ is given by

$$\frac{dN}{dt} = \frac{1}{\tau_1} \int_0^t e^{-(t-t')/\tau_1} \left[ \frac{N_0}{\tau_2} e^{-t'/\tau_2} dt' \right] . \tag{3b}$$

The expression in large parentheses gives the number of nuclei, which decay in the time interval $(t',t'+dt')$ to the first excited state. For the decay of these nuclei to the ground state, $t'$ is now the time zero, so that the emission rate is determined by the time difference $t-t'$. With the abbreviation $q=\tau_2/\tau_1$, Eq. (3b) reduces to

$$\frac{dN}{dt} = \frac{N_0}{\tau_1} e^{-t/\tau_1} \left[ \frac{1-\exp[(-t/\tau_1)(1-q)/q]}{1-q} \right] . \tag{3c}$$

The relation between the velocity at the moment of emission of the $\gamma$-ray quantum and the time elapsed since the production of the excited state can be calculated—using $dE_p(v)/dx = m dv/dt$—as

$$t(v) = \int_v^{v_0} \frac{m}{|\,dE_p(u)/dx\,|} du , \tag{4}$$

where $t=0$ is defined by the start velocity $v=v_0$ and $m$ is the mass of the projectile.

Because of this relation between velocity and time, which also connects, according to Eq. (1), the Doppler shift and time, the observed $\gamma$-ray-emission rate $dN(t)/dt$ can be transformed to the attenuated energy spectrum $dN_a(E)/dE$,

$$\frac{dN_a}{dE} = \frac{dN[t(v)]}{dt} \left| \frac{dt}{dv} \right| \left| \frac{dv}{dE} \right| . \tag{5}$$

This is valid only for a fixed angle $\vartheta$. Under the assumption that the projectiles do not change their direction during the slowing-down process, the angular distribution of the projectiles remains the same as in the case of the unattenuated spectrum. The total Doppler spectrum is then the integral over all possible angles $\vartheta$ with the weight function $F(\vartheta)$ from Eq. (2),

$$\frac{dN_a}{dE} = \int F(\vartheta) N_0 \frac{m}{\tau_1 |\,dE_p(v)/dx\,|} \times \exp\left[ -\int_v^{v_0} \frac{m du}{\tau_1 |\,dE_p(u)/dx\,|} \right] G \left| \frac{dv}{dE} \right| d\vartheta . \tag{6}$$

When the excited state at 2.3 MeV is directly populated, the function $G(v,q)\equiv 1$, otherwise $G(v,q)$ follows from Eqs. (3c) and (4) as

$$G(v,q) = \frac{1-\exp\left[ -\frac{(1-q)}{q} \int_v^{v_0} \frac{m du}{\tau_1 |\,dE_p(u)/dx\,|} \right]}{1-q} . \tag{7}$$

Hence $F(\vartheta)$ is obtained from the unattenuated spectrum, and all other terms in Eq. (6) are known except $q$ and the "stopping function" $\tau_1 dE_p/dx$. These can be determined from the analysis of the two measured attenuated Doppler spectra obtained by direct excitation of the 2.3-MeV level and by cascade feeding via the 3.9-MeV level.

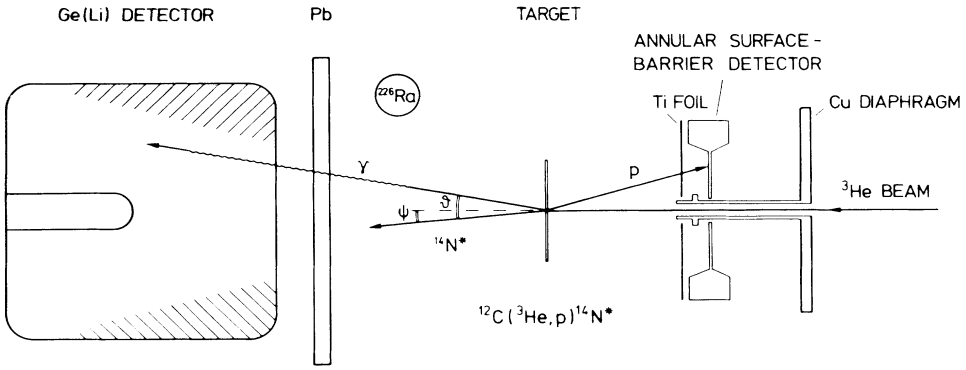


FIG. 2. Schematic diagram of the experimental setup and definition of angles (in the laboratory frame) used in the calculation of the Doppler spectra.

## III. EXPERIMENTAL DETAILS

The experimental arrangement is shown schematically in Fig. 2. A $^3$He beam was supplied by the tandem van de Graaff accelerator of the University of Cologne. After the measurement of the excitation function of the reaction $^{12}$C($^3$He,$p$)$^{14}$N*, an incident beam energy of 6.23 MeV was chosen, at which both levels at 2.3 and 3.9 MeV were reasonably strongly excited.

The targets for the unattenuated $\gamma$-ray spectra were self-supporting carbon foils with a thickness of 16.5±1.2 $\mu$g/cm$^2$, followed by a Ta beam stop 2 mm away. For the attenuated spectra the targets consisted of thin layers of carbon, evaporated onto 100-$\mu$m-thick Ni, Cu, and Ag foils, with carbon densities per unit area of 19.0±1.0, 17.2±1.0, and 11.4±1.0 $\mu$g/cm$^2$, respectively. The protons were detected in an annular Si-surface-barrier detector under backward angles between 159° and 174°. A 28-$\mu$m-thick Ti foil was used to mask the detector from backscattered $^3$He ions, while the energy straggling for the protons was still sufficiently small to resolve the peaks. At a beam current of 50 nA the count rate of the proton detector was about 1000 counts/sec. The $\gamma$ rays were detected in a Ge(Li) detector with an active volume of 100 cm$^3$ and a resolution (full width at half maximum) of 3.8 keV for 2.4-MeV $\gamma$ rays. A $^{226}$Ra source was used to provide the energy calibration of the $\gamma$-ray spectra and the detector response function. A 3-mm-thick Pb disk was placed in in front of the detector to absorb low-energy $\gamma$-ray radiation from the reaction and from the $^{226}$Ra source, keeping the total count rate with 4000 counts/sec reasonably

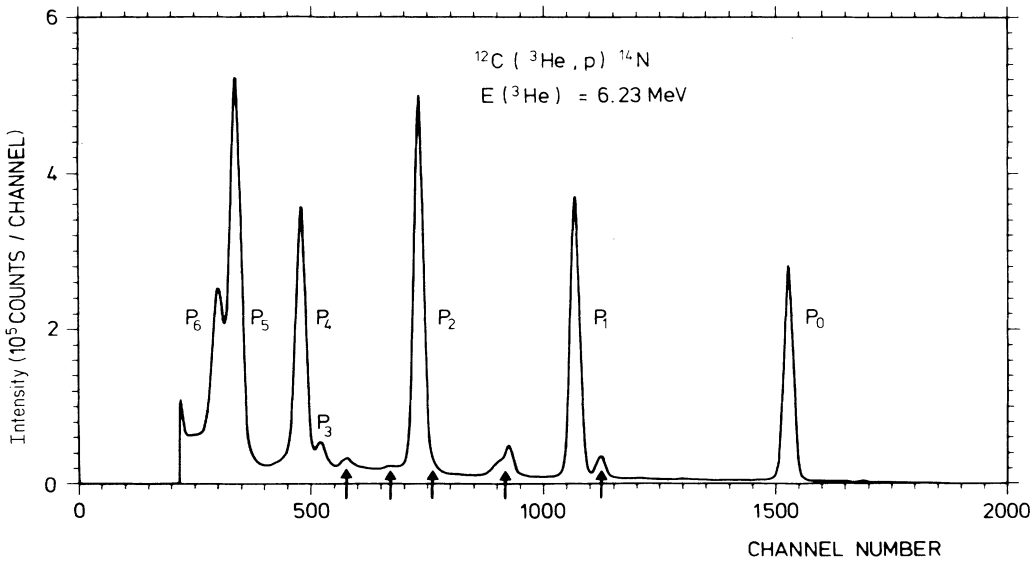


FIG. 3. Proton spectrum of the reaction $^{12}$C($^3$He,$p$)$^{14}$N* measured with the Si-surface-barrier detector. The labels $P_0, P_1, P_2 \cdots$ refer to the production of the ground state, first excited state, etc. The peaks indicated by arrows arise from the reaction $^{16}$O($^3$He,$p$)$^{18}$F*.

low. The position of the targets was changed during the measurements every three hours, in order to keep the number of produced lattice defects and the amount of implanted $^{3}$He ions as low as possible, which may have an influence on the differential energy loss of the $^{14}$N projectiles.

Coincident proton and $\gamma$-ray events were recorded in list mode using a standard fast coincidence circuit with a time resolution of about 20 nsec. $\gamma$-ray spectra in coincidence with the proton groups of interest were generated in the subsequent off-line analysis.

## IV. SPECTRA AND ANALYSIS

The proton spectrum is shown in Fig. 3. The peaks labeled $P_0, P_1, P_2, \ldots$ originate from the reaction $^{12}$C($^{3}$He,$p$)$^{14}$N*, and correspond to the proton groups from the ground state, the first excited state, etc., in $^{14}$N. The smaller bumps indicated by arrows are protons from the reaction $^{16}$O($^{3}$He,$p$)$^{18}$F* in a thin contaminant oxygen layer on the target. Figure 4(a) displays a singles $\gamma$-ray spectrum in the region near 2.3 MeV. The $\gamma$-ray spectrum in coincidence with the proton line $P_1$ [Fig. 4(b)] shows only a single line, the 2.313-MeV line of $^{14}$N, which is shifted towards higher energies due to the Doppler effect, as the projectiles move into vacuum towards the detector. This spectrum contains practically no background. The pedestal on the low-energy side is due to insufficient charge collection in the Ge(Li) detector. Figure 4(c) shows a corresponding spectrum from $^{14}$N projectiles slowed down in a Ni target.

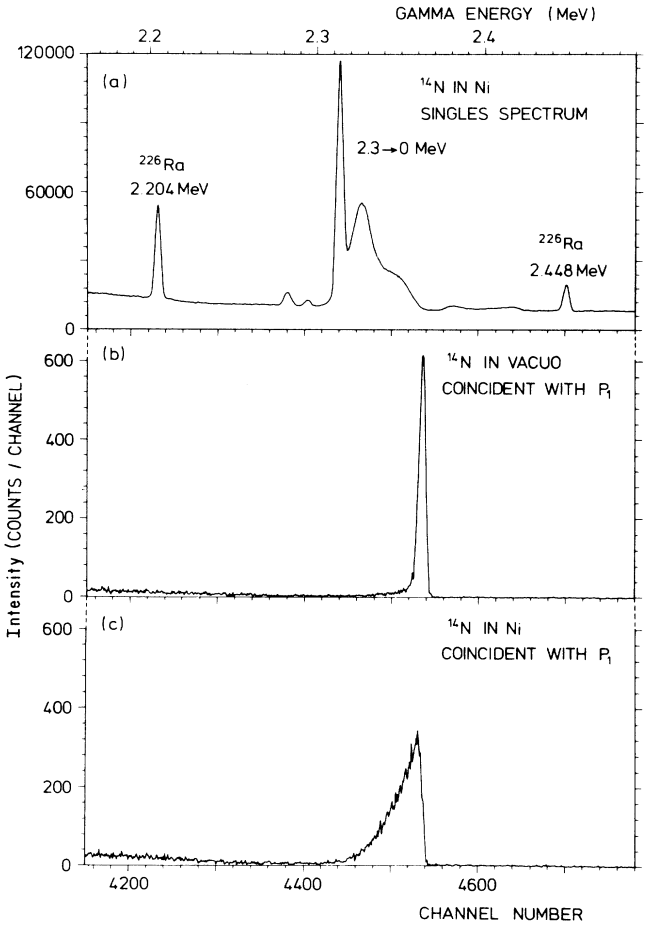


FIG. 4. Doppler spectra of the 2.3→0 MeV transition in $^{14}$N. (a) The attenuated singles $\gamma$-ray spectrum. (b) The unattenuated spectrum of $\gamma$-ray quanta coincident with the $P_1$ protons. (c) The attenuated spectrum of $\gamma$-ray quanta coincident with the $P_1$ protons.

Putting an energy window on the proton line $P_2$ gives three coincident $\gamma$-ray lines from $^{14}$N:

(1) A weak line from the direct transition 3.9→0 MeV with a branching ratio of 4%.

(2) A line at 1.635 MeV from the transition 3.9→2.3 MeV with a branching ratio of 96%.

(3) Again the line at 2.313 MeV from the subsequent transition to the ground state.

All three lines are influenced by the Doppler effect. However, the 3.948- and 1.635-MeV lines cannot be used for the evaluation, since in the first case the intensity is too low, and in the second case the line lies on the coincident Compton distribution of the 2.313-MeV line of $^{14}$N. In the energy window around $P_2$ there are also protons from the reaction $^{16}$O($^{3}$He,$p$)$^{18}$F*, where the level at 1.701 MeV in $^{18}$F is excited. The coincident $\gamma$-ray distribution, however, is far below the energy region of the investigated 2.313-MeV transition in $^{14}$N, so that the Doppler spectrum of the 2.313-MeV transition can be evaluated without background correction.

In principle, the Doppler spectra are described by Eq. (6). For a precise analysis, however, several factors which influence the spectral distribution have to be taken into account:

(1) The resolution function of the Ge(Li) detector. This was obtained from the line shapes of unbroadened $\gamma$-ray lines from a $^{226}$Ra source [see Fig. 4(a)].

(2) In the derivation of Eq. (6) it was assumed that the $^{14}$N* projectiles have a fixed start velocity $v_0$. The finite size of the particle detector leads to a certain spread in the start velocities and the recoil angles $\Psi$ (see Fig. 2). Its influence was calculated from the reaction kinematics and the known geometry.

(3) The finite size of the carbon layer in which the $^{14}$N* projectiles are produced has a twofold influence. The different locations of the production of excited projectiles and consequently different energy losses in these layers result in a further spread in the start velocities, with which the projectiles enter either the target or the vacuum. Furthermore, the different dwell times in this layer influence the relation between velocity and time in the slowing down of the excited projectiles in the target [see Eq. (4)]. This was calculated, too.

(4) During the slowing-down process in the target, the direction of the projectiles does not remain fixed, but undergoes changes due to scattering in the shielded Coulomb potential of the target nuclei. This angle straggling was estimated according to the prescription of Sigmund *et al.*[7]

(5) The effect of the energy straggling was estimated from the data of Bednyakov *et al.*[8]

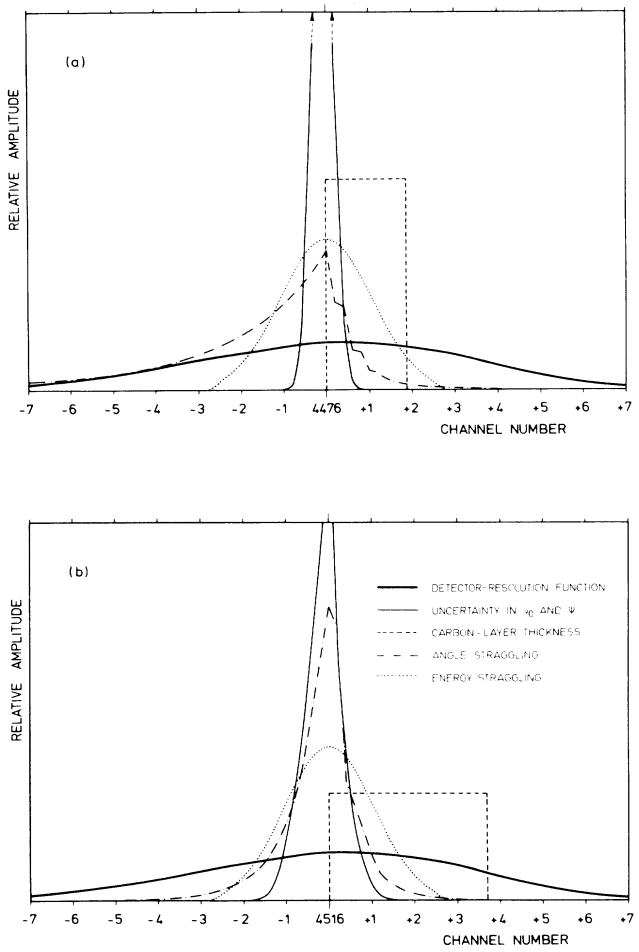


FIG. 5. Influence of the secondary effects on the attenuated $\gamma$-ray spectra at (a) 33% and (b) 75% of the maximum Doppler shift. The curves show the broadening of the $\gamma$-ray lines in comparison with the detector resolution function.

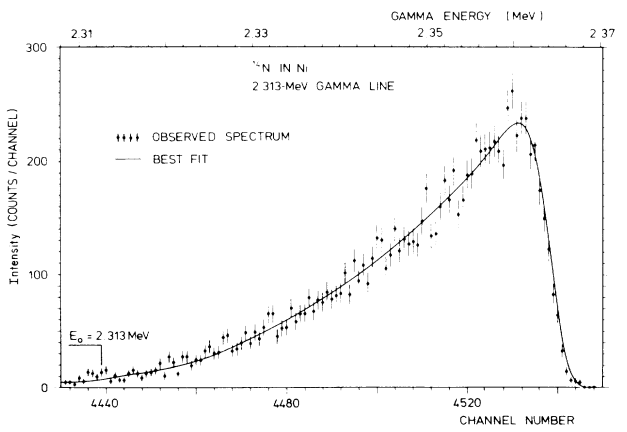


FIG. 6. Best fit to the attenuated spectrum using Eq. (6).

Figure 5 displays the results of our calculation of the effect of these factors on the $\gamma$-ray line shape at 33% and 75% of the maximum Doppler shift. The influence of the finite solid angle of the $\gamma$-ray detector, accepting different $\gamma$-ray-emission angles (see Fig. 2), is already contained in the function $F(\vartheta)$ in Eq. (6), which is determined from the unattenuated spectrum [Eq. (2)].

Finally, the attenuated Doppler spectra of the 2.313-MeV $\gamma$ rays in the two cases, i.e., direct excitation and cascade feeding via the 3.9-MeV level, were fitted in an iterative procedure to yield the product $\tau_1 dE_p/dx$ and the parameter $q=\tau_2/\tau_1$. In the fit routine the differential energy-loss ($dE_p/dx$) curve was approximated by a cubic spline function with nodes defined at $v=0.0069c$, $0.0138c$, $0.0207c$, and a zero at $v=0$. This gives the electronic component of the stopping. Nuclear stopping was calculated according to the semiempirical formula of Ziegler[9] and added to the spline function.

Figure 6 displays a fit to the observed line shape of the 2.313-MeV line for $^{14}$N ions stopped in Ni. Equally good fits were obtained for the stopping in Ag and Cu.

## V. RESULTS AND DISCUSSION

### A. Lifetimes of the states at 2.3 and 3.9 MeV

As stated above, our analysis of the line shape of the 2.313-MeV $\gamma$-ray line yielded the product $\tau_1 dE_p/dx$, where $\tau_1$ is the lifetime of the 2.3-MeV state. In order to deduce $\tau_1$, our relative curves of the energy loss in Ni and Ag were normalized to the $dE_p/dx$ value of Porat *et al.*[1] at $v=0.018c$. This is reasonable, since these au-

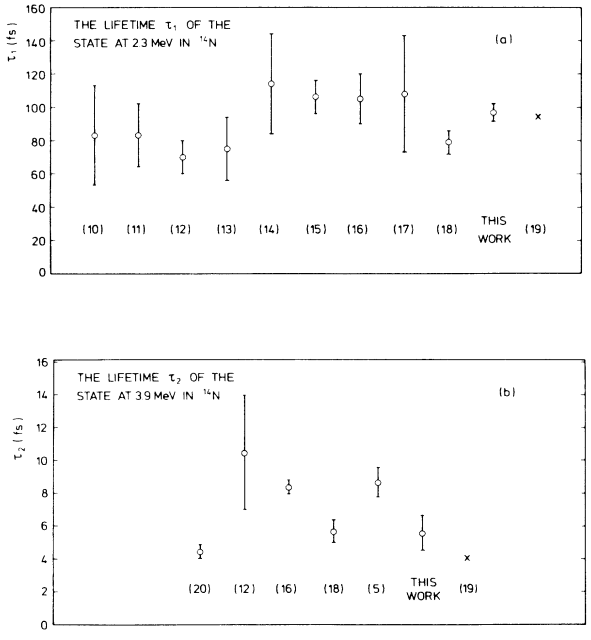


FIG. 7. Comparison of the lifetimes (a) $\tau_1$ and (b) $\tau_2$ with the measured values of various authors (Refs. 10–18, 20) (○) and calculated ones (Ref. 19) (×).

thors obtained their values in direct transmission measurements, in which the homogeneity of the foils was carefully monitored before and after transmission of the projectiles, and which delivered results of high precision (1% relative, 5% absolute).

This direct comparison yields for the lifetime of the 2.3-MeV state a value of $\tau_1 = 97.7 \pm 5.5$ fs. This value of $\tau_1$ together with the ratio $q = \tau_2/\tau_1$, obtained from the analysis of the cascade-fed 2.313-MeV line, gives for the lifetime of the 3.9-MeV state a value of $\tau_2 = 5.6 \pm 1.1$ fs. Figure 7 shows our results in comparison with previous data. They fit well in the scatter of the experimental data, but are of higher precision. They also agree quite well with calculated lifetimes.

### B. Energy loss of $^{14}$N ions in Ni, Ag, and Cu

The absolute values of the differential energy loss of $^{14}$N ions in the three stopping media investigated in the present work are shown in Fig. 8 and compared with other measurements. As mentioned in Sec. V A, the experimental data of Porat *et al.*[1] for the energy loss of $^{14}$N in Ni and Ag have been used to determine the lifetime $\tau_1$ in the product $\tau_1 dE_p/dx$, which is evaluated from the Doppler spectra. The good agreement (after the correction of the carbon layer, see below) in the general shape between our results and those of Porat *et al.*[1] shows that only one common factor, i.e., $\tau_1$, is necessary to bring the curves to coincidence. This value for the lifetime was then used to calculate absolute stopping cross sections of Cu for $^{14}$N projectiles [see Fig. 8(c)]. Also shown in Fig. 8 are experimental results of other authors, together with the semiempirical predictions of Northcliffe *et al.*[23] and Ziegler.[9]

The uncertainties of $dE_p/dx$ and lifetime values are not only determined by the statistics of the Doppler spectra, but also by the secondary effects mentioned in Sec. IV. In order to determine their contribution to the errors, we first studied how much the results are changed if we evaluated $dE_p/dx$ several times, each time neglecting a different one of these effects. This is displayed in Fig. 9. The thick solid line shows the result if all secondary effects were considered, whereas the thin solid curve is obtained if only the finite-energy resolution of the $\gamma$-ray detector is taken into account.

The influence of the angle straggling (dashed-dotted curve) is not significant at the beginning of the slowing-down process. Its disregard, however, would simulate a larger stopping power for smaller velocities. The angle straggling of $^{14}$N projectiles in the targets was calculated according to the method of Sigmund and Winterbon.[7] Their essential assumptions, however (negligible energy loss in the target and scattering angles less than about 20°), are not met in our case. Therefore, their method was modified in the following way: the range of the projectiles was numerically divided in several intervals in such a way that the necessary assumptions were individually fulfilled. By a successive convolution of the angular distributions from the corresponding layers it is also possible to calculate the angle straggling for thick targets.

If the finite thickness of the carbon foil, with which the unattenuated spectrum was measured, is neglected (dashed curve), the results are markedly changed in the high-velocity region. The same holds for the carbon layers evaporated on the carbon foils. It is obvious from Fig. 9 that none of these effects can be neglected.

The contribution to the errors can be estimated by the uncertainties with which the parameters for the correction of these effects are known (mass per unit area of the carbon foils, the energy loss of $^{14}$N in carbon, mass per unit area and density of the evaporated carbon layers). The interval size and the cutoff angle chosen in the calculation of the angle straggling also contributes to the errors; their influence can be estimated by varying these parameters.

The density of evaporated carbon layers depends strongly on the conditions during the evaporation procedure. A direct measurement of this density was not possible, therefore it had to be determined indirectly. Regarding the dotted curve in Fig. 9, it is obvious that the carbon layer on the target influences the results essentially in the high-velocity region. By adjusting the density (with known mass per unit area) to $1.4 \pm 0.2$ g/cm$^3$ it is possible to bring the results for Ni (with the largest carbon-layer thickness) into agreement with the data of Porat *et al.*[1] to within about 4%. This procedure does not disturb the determination of the lifetime $\tau_1$ because a different lifetime changes the whole curve by the same factor, whereas a different value of the density influences essentially the high-velocity part of the curve. Additionally, a further adjustment of the lifetime $\tau_1$ was still possible for the Ag target.

The total uncertainty in the value of $\tau_1 dE_p/dx$ for all three targets is about 10%, 2%, and 3.2% for velocities in the vicinity of $0.007c$, $0.014c$, and $0.021c$, respectively. The large error in the low-velocity region arises from the poor statistics (see Fig. 6) and the larger influence of the angle straggling. These errors are relative errors for $dE_p/dx$; the absolute errors should include the absolute error of 5% of the data of Porat *et al.*[1] Due to the adjustment of our $\tau_1 dE_p/dx$ curve to their $dE_p/dx$ curve this error is also the dominant one of the lifetime $\tau_1$. The overall error of $\tau_1$ is 6%, that of $\tau_2$ is 19%.

The stopping cross sections, i.e., the differential energy loss normalized to the number density $N$ of the target atoms,

$$S = \frac{1}{N}\frac{dE_p(v)}{dx} , \tag{8}$$

exhibits a strong oscillatory behavior as a function of the atomic number $Z_2$ of the targets, especially near and below the maximum of the stopping power. Maxima occur when $s$ subshells and half of the $p$ subshells are filled. Minima appear at closed subshells; they are especially pronounced for full $d$ and $f$ subshells.

All theoretical models, which describe the atoms with the Thomas-Fermi model, produce a monotonous dependence of the stopping cross sections on $Z_2$. All attempts to modify these Thomas-Fermi predictions by the use of more realistic atomic wave functions lead to this oscilla-

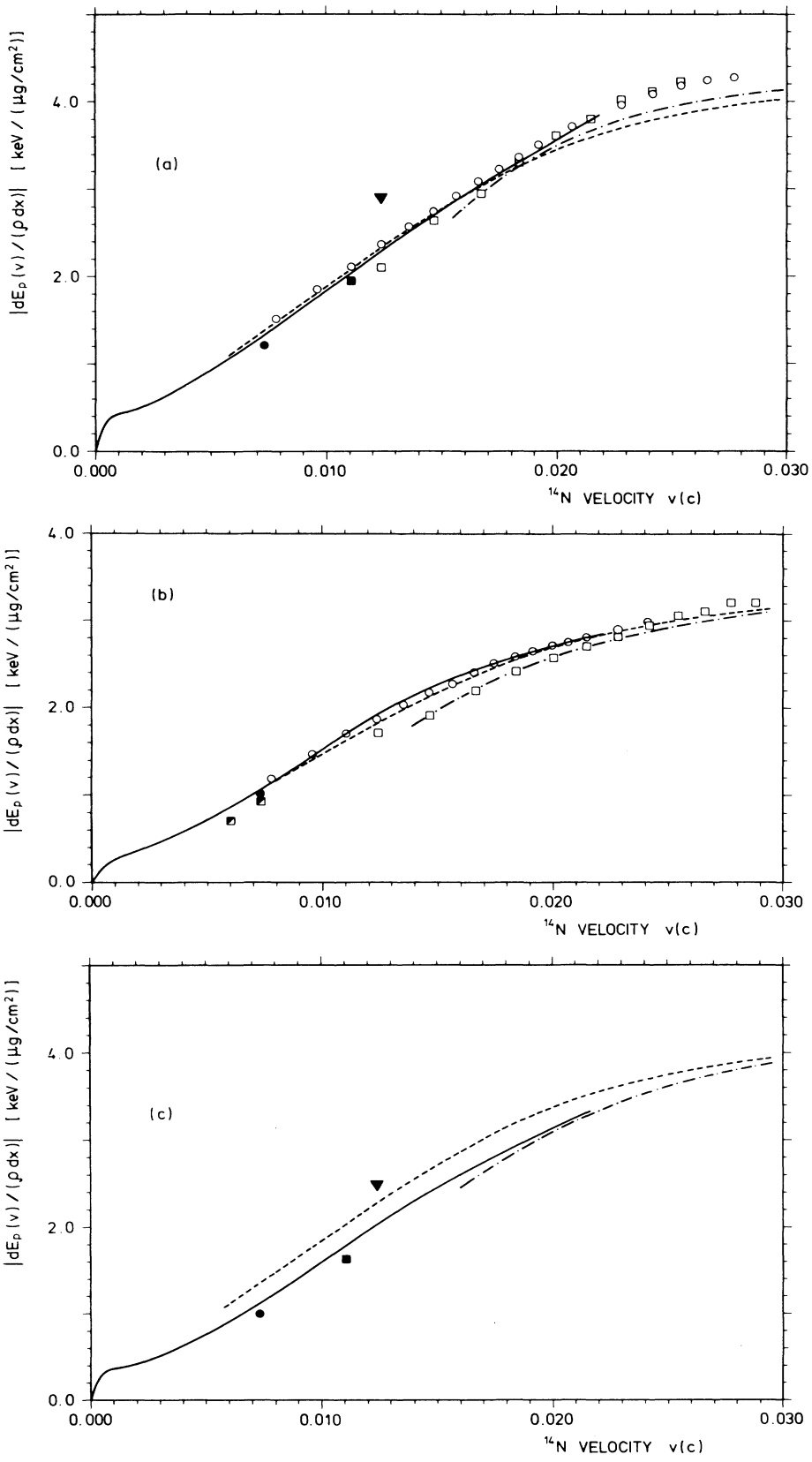


FIG. 8. Differential energy loss of $^{14}$N projectiles in (a) Ni, (b) Ag, and (c) Cu. The results of this work (——) are compared with the data of Ref. 9 (—·—·—·), Ref. 23 (— — —), Ref. 1 (○), Ref. 2 (□), Ref. 21 (▽), Ref. 22 (●), Ref. 24 (■), and Ref. 25 (◩).

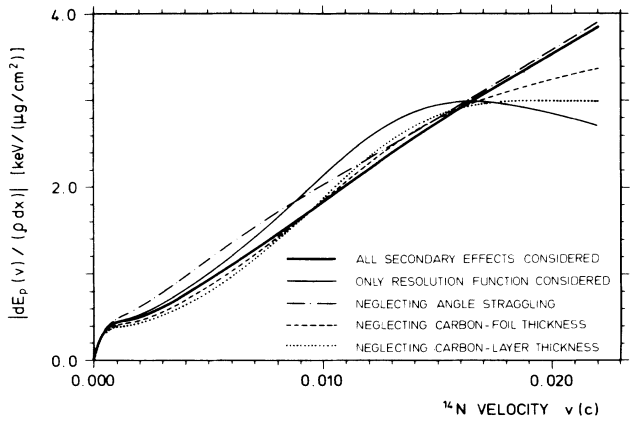


FIG. 9. Influence of the secondary effects on the energy-loss curve. The bold solid line shows the result if all secondary effects are considered. The other curves result when one or more effects are neglected.

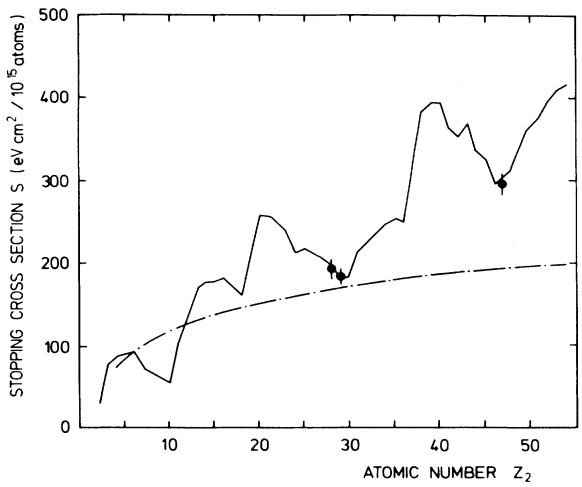


FIG. 10. Comparison of our measured stopping cross sections of Ni, Cu, and Ag for $^{14}$N at the velocity $0.011c$ with the values calculated for different target materials as a function of the atomic number $Z_2$. The dashed-dotted line is from Ref. 26 and the solid line from Ref. 22.

tory behavior of the stopping cross sections. The amplitude of the oscillations and the average slope, however, depend on the specific assumptions.

Figure 10 shows an example for each case for the stopping cross sections for $^{14}$N projectiles with a velocity of $0.011c$ as a function of $Z_2$. The dashed-dotted line is the prediction of Lindhard and Scharff,[26] based on the Thomas-Fermi model; the solid line shows the results of Land *et al.*,[22] based on a modified Firsov model.[27] The stopping cross sections of our targets Ni, Cu, and Ag should be near the minima occurring at the closure of the $3d$ and $4d$ subshells, respectively. As can be seen in Fig. 10, our results (solid circles) are very adjacent to the predictions of Land *et al.*[22]

## ACKNOWLEDGMENT

The financial support of the Bundesminister für Forschung und Technologie is gratefully acknowledged.

*On leave from the Physics Department, University of Durban-Westville, Durban 4000, South Africa.
[1]D. I. Porat and K. Ramavataram, Proc. Phys. Soc. London **78**, 1135 (1961).
[2]F. G. Neshev, A. A. Puzanv, K. S. Shyskin, E. I. Sirotinin, A. F. Tulinov, and G. D. Ved'manov, Radiat. Eff. **25**, 271 (1975).
[3]W. Neuwirth, U. Hauser, and E. Kühn, Z. Phys. **220**, 241 (1969).
[4]W. Neuwirth, W. Pietsch, K. Richter, and U. Hauser, Z. Phys. **A275**, 209 (1975).
[5]F. Ajzenberg-Selove, Nucl. Phys. **A360**, 1 (1981).
[6]P. J. Nolan and J. F. Sharpey-Shafer, Rep. Prog. Phys. **42**, 1 (1978).
[7]P. Sigmund and K. B. Winterbon, Nucl. Instrum. Methods **119**, 541 (1974).
[8]A. A. Bednyakov, Y. V. Bulgakov, V. S. Nikolaev, V. P. Sobakin, and B. M. Popov, Zh. Eksp. Teor. Fiz. **68**, 2067 (1975) [Sov. Phys.—JETP **41**, 1034 (1975)].
[9]J. F. Ziegler, Appl. Phys. Lett. **31**, 544 (1977); H. H. Anderson and J. F. Ziegler, *Hydrogen Stopping Powers and Ranges in All Elements* (Pergamon, New York, 1977).
[10]J. A. Lonergan and D. J. Donahue, Nucl. Phys. **74**, 318 (1965).
[11]K. P. Lieb, Nucl. Phys. **85**, 461 (1966).
[12]M. Bister, A. Antilla, M. Piiparinen, and M. Viitasalo, Phys. Rev. C **3**, 1972 (1971).
[13]M. J. Renan, J. P. F. Sellschop, R. J. Keddy, and D. W. Mingay, Nucl. Phys. **A193**, 470 (1972).
[14]F. Haas, R. M. Freeman, B. Heusch, S. Kohmoto, and A. Gallmann, Nucl. Phys. **A211**, 289 (1973).
[15]V. K. Rasmussen and F. R. Metzger, Phys. Rev. C **12**, 706 (1975).
[16]M. Bister, A. Antilla, and J. Keinonen, Phys. Rev. C **16**, 1303 (1977).
[17]N. Ensslin, L. W. Fagg, R. A. Lindgren, W. L. Bendel, and E. C. Jones, Jr., Phys. Rev. C **19**, 569 (1979).
[18]M. S. Antoni, A. Kiss, E. Koltay, B. Nyako, and D. Sabo, Izv. Akad. Nauk SSSR, Ser. Fiz. **44**, 1031 (1980).
[19]S. Lie, Nucl. Phys. **A181**, 517 (1972).
[20]J. W. Olness, A. R. Poletti, and E. K. Warburton, Phys. Rev. **154**, 971 (1967).
[21]K. Björkqvist and B. Domeij, Radiat. Eff. **13**, 191 (1972).
[22]D. J. Land, J. G. Brennan, D. G. Simons, and M. D. Brown, Phys. Rev. A **16**, 492 (1977); *ibid.* **22**, 68 (1980).
[23]L. C. Northcliffe and R. F. Schilling, Nucl. Data Tables A **7** (1970).
[24]D. G. Simons, D. J. Land, J. G. Brennan, and M. D. Brown, Phys. Rev. A **12**, 2383 (1975).
[25]D. Ward, H. R. Andrews, I. V. Mitchell, W. N. Lennard, and R. W. Walker, Can. J. Phys. **57**, 645 (1979).
[26]J. Lindhard, M. Scharff, and H. E. Schiott, K. Dan. Vidensk. Selsk. Mat. Fys. Medd. **33**, No. 14 (1963).
[27]O. B. Firsov, Zh. Eksp. Teor. Fiz. **36**, 1517 (1959) [Sov. Phys.—JETP **9**, 1076 (1959)].